Journal of Membrane Science 534 (2017) 73–82

Contents lists available at ScienceDirect

Journal of Membrane Science

journal homepage: www.elsevier.com/locate/memsci

Electrospun ultrafine fibrous PTFE-supported ZnO porous membrane with self-cleaning function for vacuum membrane distillation

Qing-Lin Huang*, Yan Huang, Chang-Fa Xiao, Yan-Wei You, Chao-Xin Zhang

State Key Laboratory of Separation Membranes and Membrane Processes, Department of Material Science and Engineering, Tianjin Polytechnic University, Tianjin 300387, China

ARTICLE INFO

Keywords:
PTFE/ZnO ultrafine fibrous membrane
Electrospinning
Photocatalysis
VMD
Self-cleaning

ABSTRACT

In this work, novel photocatalytic porous membranes consisting of ZnO supported by a poly(tetrafluoroethylene) (PTFE) substrate were fabricated by sintering electrospun PTFE/poly(vinylalcohol) (PVA)/zinc acetate dehydrate composite membranes after removal of the PVA carrier. The rheological properties of spinning solution were investigated. Results showed that the spinning solution exhibited good electrospinning performance and the membranes exhibited excellent flexibility, high chemical stability, and a highly specific surface area. The photocatalyst-ZnO particles derived from the thermal decomposition of zinc acetate dehydrate were homogeneously immobilized on the surface of ultrafine PTFE fibers to avoid the influence of agglomeration and sedimentation when ZnO particles were added directly. The performances of PTFE/ZnO membranes were investigated in vacuum membrane distillation (VMD) with photo-degradation experiments. Results indicated that appropriate PTFE/ZnO membranes could be an effective way for salt rejection and dye removal at the same time. In the VMD with photo-degradation experiments, the salt rejection was up to 99.70% and the dye removal rate of feed solution was up to 45% after 10-h operating time. Meanwhile, the PTFE/ZnO membranes also showed good self-cleaning ability. The fouled membranes could be cleaned after the 3-h UV irradiation with a permeate flux recovery rate of more than 94% after UV irradiation cleaning for 3-h. The immobilization of ZnO on substrate of ultrafine fibrous PTFE porous membranes may provide a wide range of potential applications for the treatment of dye-containing effluent.

1. Introduction

Environmental contamination related to release of toxic organic waste into waters is an important global issue with rapid population growth, industrialization, and long-term droughts. Contaminated water can have serious implications on human health and this issue is only expected to become worse in the coming decades [1–3]. Membrane technology as an energy-saving, environmental friendly method offers great potential in the water/wastewater, pharmaceutical, bioengineering, chemical, and electronic industries [4,5]. Vacuum membrane distillation (VMD) is one type of membrane distillation (MD) configurations, where the pressure difference across the membrane acts as the driving force for trans-membrane vapor flux, while a hydrophobic microporous membrane acts as the medium [6]. Compared with traditional separation technologies, as well as other pressure-driven membrane separation processes, VMD has the advantages of low energy consumption and nearly 100% rejection, the ability to condense the non-volatile agent while removing volatile organic agents in the water solution [7,8]. However, the scaling, organic fouling and wetting phenomena in VMD, which results in a sharp decline in the membrane flux and shortens the membrane's lifespan, have been the major challenge to VMD implementation [9]. Multiple strategies have been employed in order to inhibit membrane fouling for VMD, including pretreatment of the feeding solution, membrane flushing, gas bubbling, surface modification to create an anti-fouling membrane, photo-catalysis and so on [10–12]. Perfluorinated polymers have been studied extensively for MD due to their superior thermal and chemical stability, corrosion resistance, and exceptional abilities to separate fine particles under harsh conditions [13–15].

Photocatalytic oxidation of wastewater treatment using semiconductor materials is an emerging water treatment technology. Compared with the traditional water treatment technologies, it is considered a particularly promising water treatment technology due to its adaptability towards organic pollutants, relatively low environmental impacts, ability to be conducted under ambient temperature and pressure, and natural energy source (sunlight) [16,17]. Since the 1970s, heterogeneous photocatalysis has been successfully applied to degrade harmful molecules [18,19]. Photocatalytic membrane reactors (PMRs) are

* Correspondence to: Tianjin Polytechnic University, No. 399 West Binshui Road, Xi Qing District, 300387 Tianjin, China.
E-mail address: huangqinglin@tjpu.edu.cn (Q.-L. Huang).

http://dx.doi.org/10.1016/j.memsci.2017.04.015
Received 17 January 2017; Received in revised form 9 April 2017; Accepted 11 April 2017
Available online 12 April 2017

hybrid reactors in which photocatalysis is coupled with a membrane process. In suspended PMRs, the catalyst particles are uniformly dispersed in the wastewater. However, the post-separation of the catalyst particles after water treatment remains a major obstacle in achieving higher efficiency and applicability in industrial processes. Immobilized PMRs are loaded onto the membrane surface or entrapped in the membrane to produce a composite membrane which plays the role of both a catalyst and a selective barrier against contaminants of interest [20,21]. Photocatalysts offer the main advantage that they do not lead to extensive membrane fouling.

Zinc oxide (ZnO) has been studied for use in optoelectronics applications owing to its direct wide band gap (Eg~3.3 eV at 300 K) and large exciton binding energy (60 m eV) at room temperature. Drawbacks related to catalyst separation and recovery may be overcome by using various supports, including glass mats, inorganic carbon fabrics, indium tin oxide (ITO) glass, synthetic fabrics, plastics, stainless steel, and zeolites, as a substrate to grow ZnO nanostructures [22,23]. However, in practical application, the following characteristics of the polymers make them especially suited for use as a support: 1) harmless materials which are chemically inert and mechanically stable with high durability, 2) hydrophobicity, which provides the added advantage of increasing the efficiency of adsorption and subsequent oxidation on the surface, 3) high UV resistance and oxidation resistance by oxidative radicals, and 4) relatively easy processing into desired shapes [24,25].

Electrospinning has proven to be an effective, straightforward, and convenient method to synthesize continuous structures sub-micron in diameter, as well as nanoscale polymers and semiconductor metal oxide fibers [26,27]. It may also permit the permeation of water, which is favorable for water purification applications [28]. Prior studies have found that nanofibrous photosensitive semiconductor materials (e.g., TiO_2, ZnO) outperformed nano-particles in the photocatalytic degradation of organic dye molecules, which may be attributed to the porous nature of the nanofibers [29–31]. To build upon the previous work, a more detailed evaluation of methods to increase the uniform dispersion for the catalysts and obtain satisfactory recycling processes is required. The immobilization of photocatalyst in the membrane is possibly an applicable approach, since it could not only overcome the difficulty of post-separation of photocatalyst particles, but also integrate membrane separation and photocatalytic degradation of contaminants in a single membrane device.

In this study, the highly flexible PTFE/ZnO ultrafine fibrous porous membranes were fabricated by a simple combination of electrospinning and sintering processing to increase the uniform dispersion for the catalysts and obtain satisfactory recycling or reuse processes. ZnO particles were homogeneously immobilized on the surface of PTFE ultrafine fibers via thermal decomposition of PTFE/PVA/zinc acetate in an air atmosphere and a two-step dipping and chemical deposition technique. The flexibility and high surface area of polymeric nanofibers were then utilized for the growth of photochemically active ZnO. The photocatalytic decomposition of dyes in wastewater effluent was evaluated using Rhodamine B (RhB) as a model contaminant with ultraviolet light. The self-cleaning performances of PTFE/ZnO membranes were investigated by discussing the rejection and permeate flux recovery in vacuum membrane distillation (VMD) under UV irradiation experiments.

2. Experimental methods

2.1. Materials

An aqueous dispersion of PTFE (FR301B) was purchased from 3F New Materials Co., Ltd. (Shanghai, China). Poly(vinyl alcohol) (PVA, Type1788, degree of polymerization 1700, and degree of alcoholysis 88%) was obtained from Lanbo Industrial Co., Ltd., (Hangzhou, China). Poly(acrylonitrile) (PAN, degree of polymerization 50,000) was purchased from Qilu Petrochemical Technology Co., Ltd., (Shandong, China). Zinc acetate, sodium hydroxide (NaOH), polyethylene glycol 6000 (PEG 6000) and N,N-dimethylformamide (DMF) were purchased from Guangfu Fine Chemical Research Institute (Tianjin, China). And all of them had analytical grade. All the reagents were used as received without further purification.

2.2. Membrane preparation

2.2.1. PTFE/PVA/zinc acetate dehydrate composite membranes

A 10 wt% aqueous solution of PVA was prepared by dissolving PVA powder in distilled water at 80 °C under constant agitation for at least 6 h. After the solution was cooled to 25 °C, an aqueous dispersion of PTFE and zinc acetate dehydrate was added to the PVA solution under constant stirring for 3 h to form a precursor spinning solution containing zinc acetate at 0 (S-0), 10 (S-10), 20 (S-20) and 30 wt% (S-30), respectively. PAN was dissolved in DMF to make a 10 wt% solution. Based on results from our previous work, a PTFE/PVA mass ratio of 6:1 was chosen to produce a uniform fiber diameter and distribution [32].

The electrospinning apparatus consisted of a syringe feeder system, a metallic ground fiber collector, and a variable high-voltage power supply connected to the needle tip (0.34 mm inner diameter) of the syringe, all of which were housed in a temperature-controlled room (25 °C). Electrospinning was performed at an applied voltage of 25 kV, a spinning distance of 10 cm, and a fluid flow rate of 0.008 mL/min, which resulted in a dense web of the electrospun PTFE/PVA/zinc acetate dehydrate composite membranes.

2.2.2. PTFE/ZnO membranes

To increase the structural integrity of the as-spun membranes, post-heat treatment was carried out in a vacuum oven at 60 °C for 3 h. Then the as-prepared composite fibers were subjected to high-temperature calcination (300 °C up to 380 °C for 10 min) to obtain PTFE/ZnO membranes (referred to as Technique 1). The same procedure was adopted for the formation of ZnO particles. An enhanced photocatalytic membrane was also prepared by a two-step dipping and hydrothermal method (Technique 2), which had been described previously [33–35]. The membranes were treated for 30 min in a solution of 0.05 mol/L NaOH, and then washed with distilled water and dried at room temperature. The treated membranes were then dipped in a sealed chemical bath containing an equimolar mixture of zinc acetate (0.1 mol/L), NaOH (1 mol/L), and PEG 6000 (0.015 mol/L). Finally, the samples were sintered and rinsed several times with deionized water, and then heated at 150 °C for 30 min to vaporize any organic deposits. A schematic showing the preparation of ultrafine fibrous PTFE/ZnO porous membranes is shown in Fig. 1. Names and properties of the membranes are given in Table 1.

2.3. Characterization

The rheological behavior of the PTFE/PVA/Zinc acetate spinning solutions was investigated with a rheometer (HAAKE MARS, Thermo Fisher Scientific, USA). Shear stress was measured over a range of shear rates (γ) from 1 to 1000 s^{-1} for each sample. The temperature of spinning solution was 25 °C. The morphology of the membranes was evaluated by scanning electron microscopy (SEM; FESEM S4800, and SEM TM3030, Hitachi, Japan) and atomic force microscopy (AFM, CSPM 5500, China). Contact angle measurements were performed using an optical contact angle meter (model DSA100, KRUSS Co., Germany) by the sessile drop method of water drops. The measurements were conducted in room temperature (25 °C) and at a relative humidity of 40–50%. The droplet was left on the membrane surface for 60 s before recording. X-ray photoelectron spectroscopy (XPS) measurements were conducted using a K-Aepna XPS system (Thermo Fisher, USA). The presence of ZnO particles was evaluated by X-ray diffraction (XRD, D8 Discover, Bruker, USA) and an energy dispersive X-ray detector (EDX, Ameter, USA). The thermal degradation of the membrane samples was

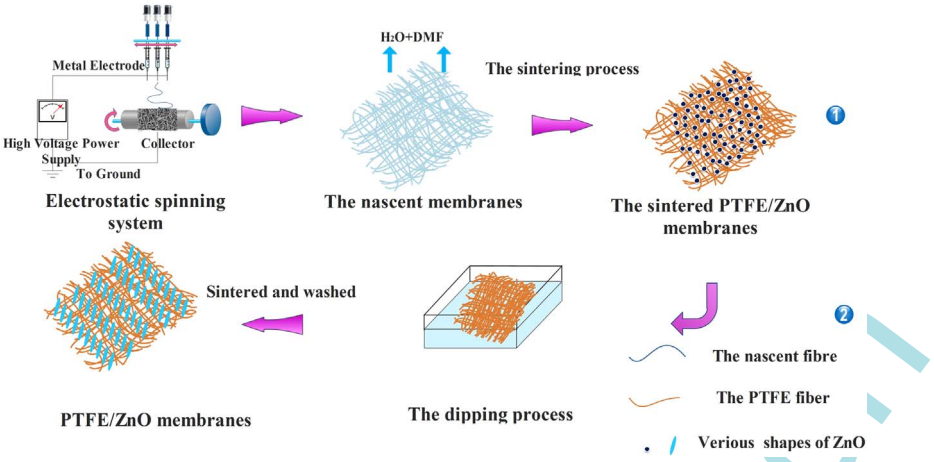

Fig. 1. Schematic illustration of the ultrafine fibrous PTFE/ZnO porous membranes preparation process.

Table 1
The sample names of ultrafine fibrous porous membranes.

The addition of zinc acetate (wt %)	Sample name		
	The nascent membranes	The sintered membranes (technique 1)	After dipping and sintering (technique 2)
0	M-p 0	M-s 0	–
10	M-p10	M-s10	–
20	M-p20	M-s20	M-d20
30	M-p30	M-s30	–

assessed using a thermogravimetric analysis instrument (TA-SDT Q600, USA) under an air atmosphere at a heating rate of 5 °C/min from room temperature to 800 °C (membrane sample weights ranged from 6 to 10 mg) UV–visible absorption spectra of ZnO nanoparticles and prepared membranes were collected using a spectrometer (UV WinLab V6, Perkin Elmer, USA). The tensile strength of membranes was determined at room temperature using an electronic tensile tester (JBDL-200N, China) at a tensile rate of 2 mm/min. The specific surface areas of the samples were determined from N_2 adsorption–desorption isotherms by the BET method (Autosorb-iQ, Quantachrome, USA). The membrane porosity and pore diameter distribution were determined by mercury injection (IV9510, Micromeritics, USA). The membrane liquid entry pressure (LEP) was determined using a laboratory device at room temperature as described in literature [36,37].

2.4. Membrane distillation with photo-degradation assay

Photocatalytic experiments were conducted to assess the degradation of RhB in feed solution. The separation performance of the membranes was tested in VMD experiments. As shown in Fig. 2, the VMD experiment was conducted in a lab scale custom-made filtration unit. The feed solution was pre-heated before it was circulated to one side of the membrane. Cell dimensions and the effective membrane area surface were 113.10 cm^2 and 45.36 cm^2, respectively. The membrane module (made by quartz glass) and the membrane surface were exposed under UV irradiation (500 W high pressure mercury lamp with a maximal emission at approximately 365 nm). Hot feed solution (80 °C feed temperature) was pumped to the feed side of the membrane by a diaphragm pump at a constant flow rate of 1.5 L/min. A vacuum was applied using a vacuum pump to the other side of the membrane. The permeate vapor was condensed and collected as the product.

The VMD permeate flux was calculated by Eq. (1) :

$$J = \frac{V}{T \times A} \quad (1)$$

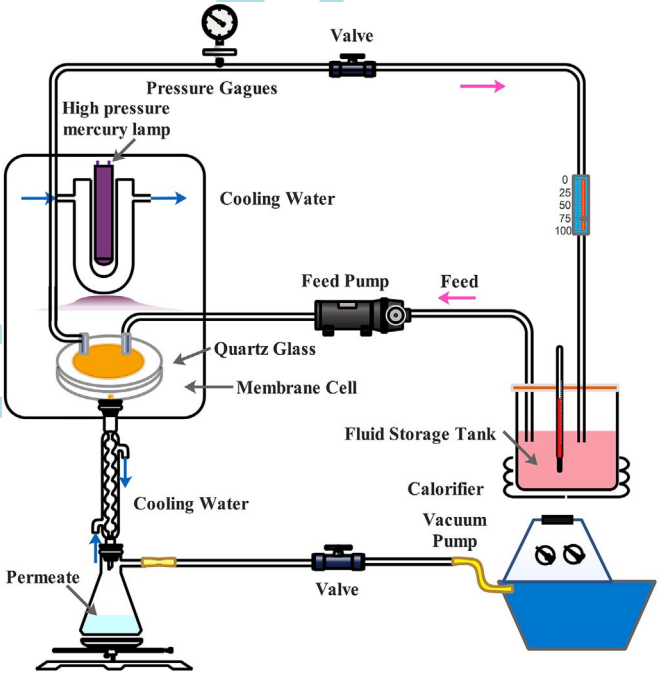

Fig. 2. Schematic diagram of VMD with photo-degradation experiment.

where J is the permeation flux (L m^{-2} h^{-1}), V is the volume of the solution in the permeate side (L), T is the running time (h), and A is the effective membrane area (m^2).

The conductivity of the feed solution and the permeate water was measured by a conductivity meter (ST10C-B, OHAUS), and the concentration was calculated by the linear relationship between the conductivity and concentration, which was described elsewhere [37,38]. The photo-degraded sample was removed from the reaction system and centrifuged. Concentrations of RhB were analyzed using a TU-1810 UV–vis spectrophotometer (Beijing Purkinje General Instruments, China) with absorbance measured at 554 nm, at which the maximum absorption occurs. The salt or dye rejection R was calculated by Eq. (2):

$$R = \left(1 - \frac{C_p}{C_f}\right) \times 100\% \quad (2)$$

where C_f and C_p are the concentration of the feed solution and permeate water, respectively.

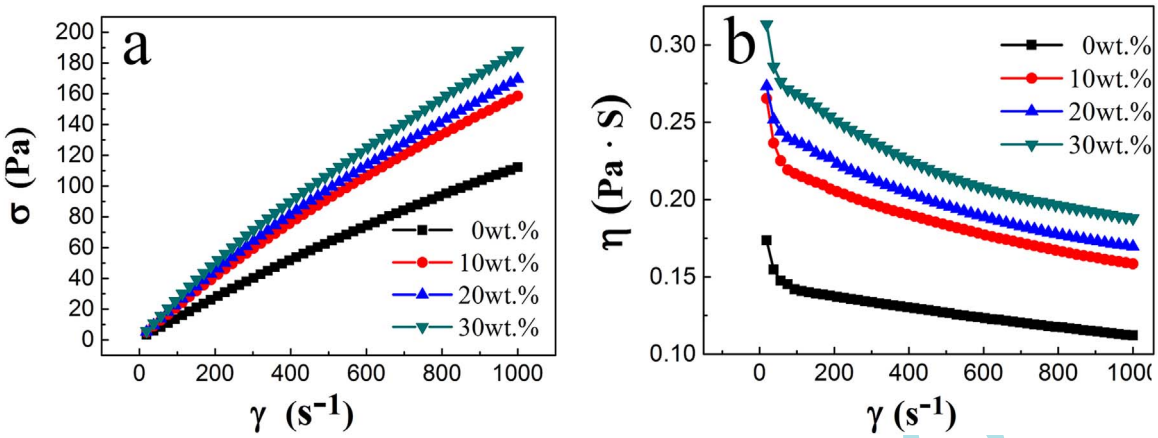

Fig. 3. Effect of addition of zinc acetate on σ-γ curve (a) and η-γ curve(b).

3. Results and discussion

3.1. Rheological properties

Rheological measurements can be used to describe the structural characteristics of polymer solutions, including the molecular state and gelation behavior [39,40]. The rheological properties of spinning solutions also strongly affect their wet spinning and electrospinning performance. The effect of addition of various amounts of zinc acetate on the rheological behavior of the PTFE/PVA/zinc acetate spinning solutions is shown in Fig. 3. The shear stress (σ) of the PTFE/PVA/zinc acetate spinning solutions was found to be higher than that of the PTFE/PVA solutions at the same shear rate (γ). The incorporation of zinc acetate increased the viscosity (η) of spinning solutions at loading levels as low as 10 wt%. The shear stress and viscosity continuously increased with an increase in the amount of zinc acetate. To further investigate the effects of zinc acetate concentration on the non-Newtonian behavior of spinning solutions, shear stress was plotted against shear rate. The non-Newtonian index (n) was observed to decrease with an increase in zinc acetate (Table 2). When the addition of zinc acetate was 20 wt%, the value of n reached a maximum of 0.8702 which suggests that the spinning solution still exhibited good Newtonian flowing properties. Taken together, these results indicate that the spinning solutions were stable during the electrospinning process.

It can be seen that the viscosity of the spinning affects the dimension of the nascent nanofibers, and thicker nanofibers can be obtained by high viscosity spinning solutions as shown in Fig. 4. Moreover, a low viscosity spinning solutions can make membranes with smaller pore sizes for that the pores formed by thinner nanofiber intertwined should be smaller than by the nanofibers with larger diameters [41,42].

3.2. Morphology

SEM images and the corresponding histograms of the fiber diameter distribution of the nascent and sintered membranes are shown in Fig. 4. The PTFE/PVA composite fibers (Fig. 4**a**) were observed to be uniform in diameter, indicating that the parameters used in the electrospinning process were appropriate. Based on the histogram (Fig. 4), the fiber diameter increased with increasing zinc acetate and spinning solution viscosity. It can be seen that electrospun fibrous membranes are usually porous, which enables the construction of an open three-dimensional network. This network offers a high surface area and flexible surface functionalities that can act as either substrates or precursors for obtaining the desired nanostructures.

After the sintering process, the decrease in the fiber diameter and the concurrent coarsening of the fiber surface may be attributed to the densification of PTFE fibers and the removal of the polymer and organic components in the nascent fibers. Although the fiber diameter was reduced after the sintering process, the fibers remained dense and fibrous. Meanwhile the photocatalyst-ZnO particles derived from the thermal decomposition of zinc acetate dehydrate were homogeneously immobilized on the surface of ultrafine PTFE fibers after the sintering process. In addition, increase in zinc acetate dehydrate contents resulted in a significant increase in the quantity of ZnO particles.

The surface morphologies of the membranes were also evaluated by AFM. The three dimensional (3D) images are shown in Fig. 5 and the roughness parameters of the surfaces of the membranes are presented in Table 3. The surface roughness of the PTFE/ZnO membranes was considerably higher than that of the PTFE membranes, which was caused by the ZnO immobilized on the surface of ultrafine PTFE fibers.

Table 2
The Non-Newtonian index of different spinning solutions.

Temperature (°C)	Spinning solution	S-0	S-10	S-20	S-30
25	Non-Newtonian index n	0.9023	0.8751	0.8702	0.8598

3.3. Physical characteristics of PTFE/ZnO membranes

High optical absorbance is essential for effective photocatalysis. UV–vis absorption was used to study the optical properties of the synthesized ZnO. The UV–vis adsorption spectra of different samples are shown in Fig. 6**(a)**. It is clearly seen that the UV–vis absorption spectra of ZnO nanoparticles shows an absorption edge at about 390 nm and the absorption edges of PTFE/ZnO membranes do not show obvious red shift or blue shift. After loading with ZnO, PTFE/ZnO membranes showed a larger enhancement absorption in the visible range as compared to pure ZnO nanoparticles. The absorbance in the visible region was found to increase as zinc acetate increased.

The prepared membranes were evaluated by TG to better understand their thermal stability and decomposition temperature. As shown in Fig. 6**(b)**, the PVA showed initial signs of degradation at a. 240 °C, while the PTFE membrane began to decompose at ca. 530 °C. There was no discernible difference in the initial decomposition temperature between PTFE/PVA nascent membrane and the PTFE/PVA/ zinc acetate nascent membrane, which suggests that both membranes exhibited good thermal stability. Compared with the TG pattern of M-s0, the process started with a weight loss of the thermal dehydration of zinc acetate dehydrate, and further decomposition of anhydrous zinc acetate caused a weight loss within the temperature region of 150–280 °C [43]. There was a minimal change in weight loss after ca. 680 °C, suggesting that a small amount of ZnO remained in the reactor.

The XRD pattern of prepared membranes and ZnO nanoparticles is shown in Fig. 6**(c)**. Compared with the XRD curve of the M-s0, the XRD curve of PTFE/ZnO membranes showed the presence of additional

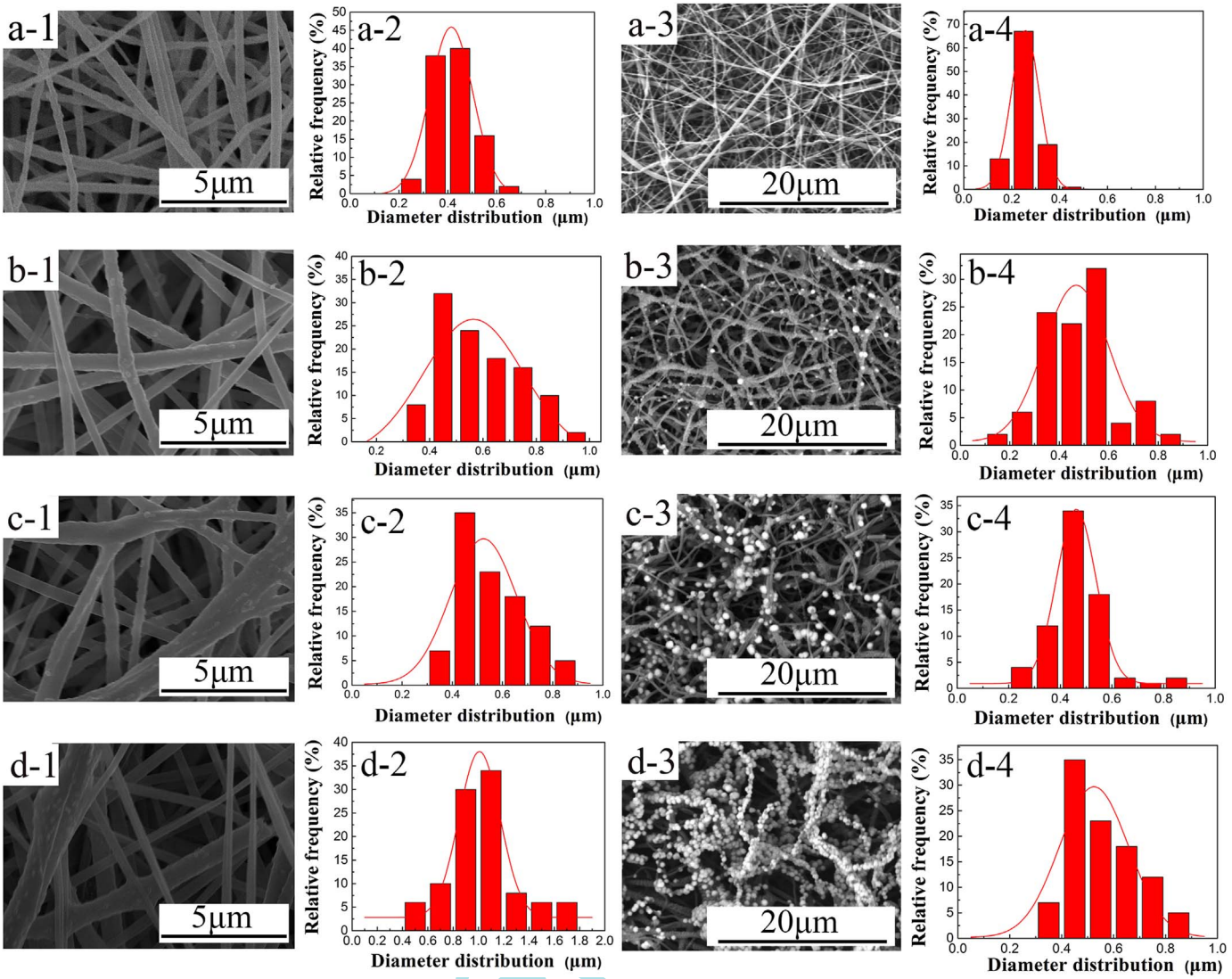

Fig. 4. SEM images and the corresponding histograms of the fiber diameter distribution of the nascent and sintered membranes (a-1: M-p0; b-1: M-p10; c-1: M-p20; d-1: M-p30; a-3: M-s1; b-3: M-s10; c-3: M-s20; d-3: M-s30).

diffraction peaks at 2θ = 31.7° (100), 34.3° (002), 36.2° (101), and 47.2° (102), corresponding to a pure ZnO crystalline phase [44]. These results together confirm that the product immobilized on the surface of ultrafine PTFE fibers was ZnO.

The XPS survey scan (Fig. 7) shows the expected signals from Zn (2p3), F (1s), O (1s) and C (1s). In addition to C1s, O1s, and F1s peaks observed at ca. 285, 532, and 692 eV, respectively, there is also a distinct peak attributed to Zn2p3 at ca. 1023 eV which are close to the data for Zn (2p) in ZnO. On the other hand, we find that Zn2p peak is sharp, as demonstrated that there is $Zn2+$. The Zn2p3 peak shifted to a

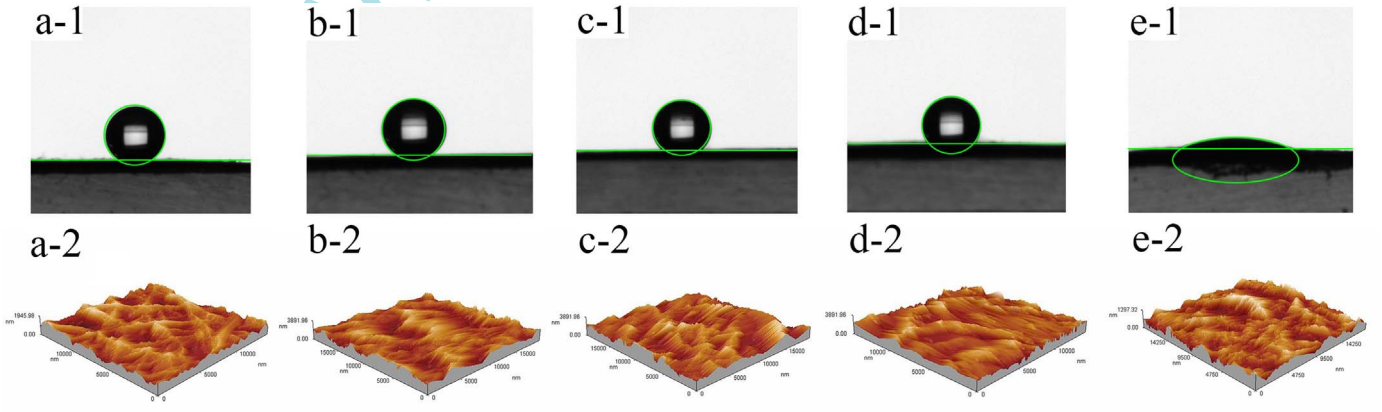

Fig. 5. WCA images (1) and 3D AFM images (2) of the PTFE/ZnO membranes (a: M-s0; b: M-s10; c: M-s20; d: M-s30; e: M-d20).

Table 3
The properties of PTFE/ZnO membranes.

Samples	BET-specific surface area (m^2/g)	Roughness average (nm)	WCA (deg.)	Porosity (%)	Liquid entrance pressure (MPa)	Mean pore size (nm)	Mechanical strength (MPa)
M-s0	22.558	188	156.6 ± 1.7	67.95	0.19 ± 0.02	465	3.13 ± 0.12
M-s10	7.091	338	148.2 ± 0.9	72.47	0.15 ± 0.03	668	1.93 ± 0.18
M-s20	7.558	319	138.3 ± 0.2	73.58	0.12 ± 0.01	549	1.70 ± 0.27
M-s30	9.942	297	117.9 ± 1.9	71.05	–	1034	–
M-d20	10.592	169	10.3 ± 0.7	67.21	–	426	1.16 ± 0.13

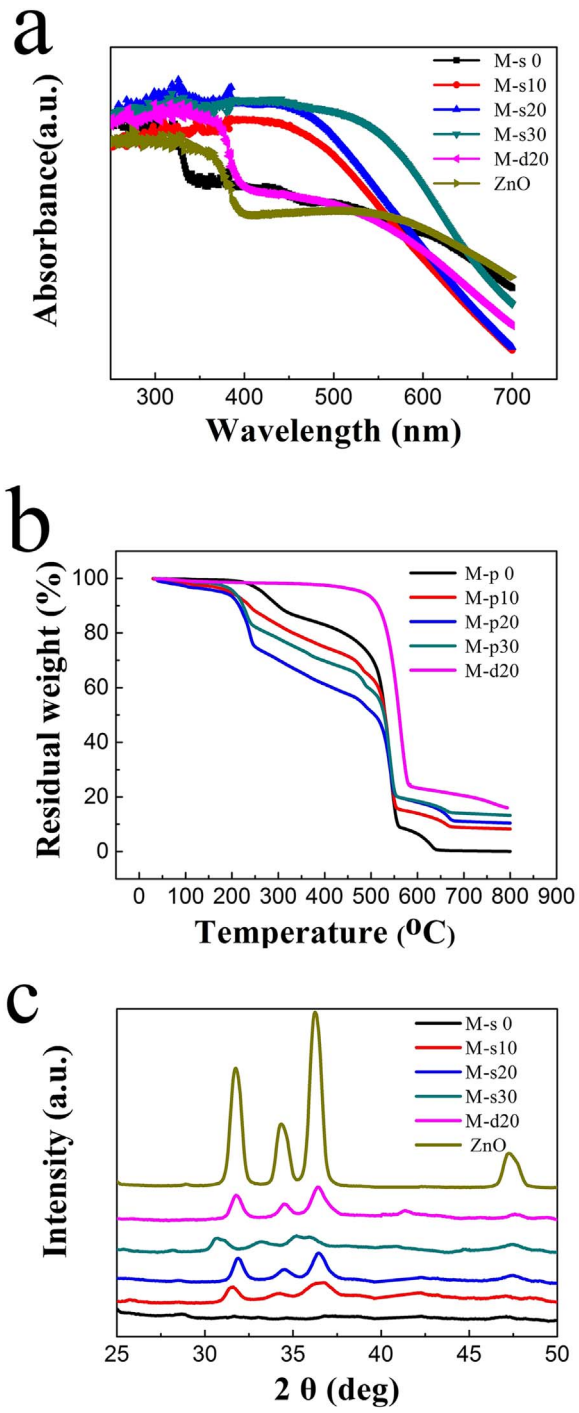

Fig. 6. UV–visible absorption spectra (a), TGA diagram (b) and XRD pattern (c).

higher energy value, indicative of the dipping and sintering process which increasing the loading of ZnO. The peaks at 1022 and 1046 eV in the spectrum corresponding to the doublet of Zn (2p3/2) and (2p 1/2), respectively, can be attributed to the formation of hexagonal ZnO nanorods [45].

Nanofibers or ultrafine fibers entangle in a matrix to form the membrane. In general, the pore size of membranes is similar to the size of nanofibers or ultrafine fibers [46]. Electrospun membranes constructed of randomly assembled fibers have been shown to exhibit more controllable membrane parameters, including porosity and pore size values [41]. All of the prepared membranes possessed relatively high porosity above 67% and a relatively high BET specific surface (Table 3). Meanwhile, the mean pore size value and LEP value were suitable for M-s10 and M-s20 to bear the vacuum or pressure applied. M-s30 is not suitable for application due to its poor mechanical properties and relatively large membrane pore size caused by uneven fiber diameter.

3.4. Effects of the two-step dipping and sintering

In order to enhance the photocatalytic activity, an enhanced photocatalytic membrane was also prepared by a two-step dipping and hydrothermal method to increase the loading of ZnO particles. In addition, the experiments of photo-degradation of dye-containing water treatment and recovering photocatalyst require the membrane should not only have sufficient mechanical strength but also high photocatalyst (ZnO) loading. It can be seen that M-s30 exhibited poor mechanical strength and low LEP value (Table 3), which was unsuitable for the vacuum or pressure applied during in the VMD process. Moreover, compared to M-s10, M-s20 turned to own a higher ZnO loadings according to a series of tests (TGA、XRD and EDX in Supplementary material), which could have a higher efficiency of photo-degradation. Therefore, M-s20 was chosen for further dipping and sintering processing (Technique 2, M-d20).

As shown in Fig. 8, after the processing, an uniform ZnO coating was observed by SEM. The surface of PTFE fibers became coarse and bumpy, which indicates the presence of ZnO on the surface. The results of characterization above (Fig. 6 and Fig. 7) confirmed that together. To some extent, the two-step dipping and sintering processing resulted in a significant increase in the quantity of ZnO crystals. Meanwhile, we noticed that the dipping process would reduce the roughness of PTFE membrane which further led to a low WCA and LEP values."

3.5. Photocatalytic activity and stability of PTFE/ZnO membranes

The photocatalytic performance of PTFE/ZnO membranes was investigated by measuring the removal efficiency and color change of RhB solution under UV irradiation (Fig. 9). The absorption spectra during the direct photolysis time clearly showed a decrease in the characteristic RhB absorption bands (Fig. 9**a-b**). After exposure to UV irradiation for 4 h, the M-d20 and M-s20 membranes were able to degrade 97.8% and 93.3% of the RhB respectively, whereas the RhB was only self-photolysis degraded by 15.4%. For M-d20 and M-s20 membranes, the RhB dye was almost completely degraded after 5 h exposure. As shown in the inset of Fig. 9**c**, with PTFE/ZnO membranes as the photocatalyst, there was obvious color change of RhB solution

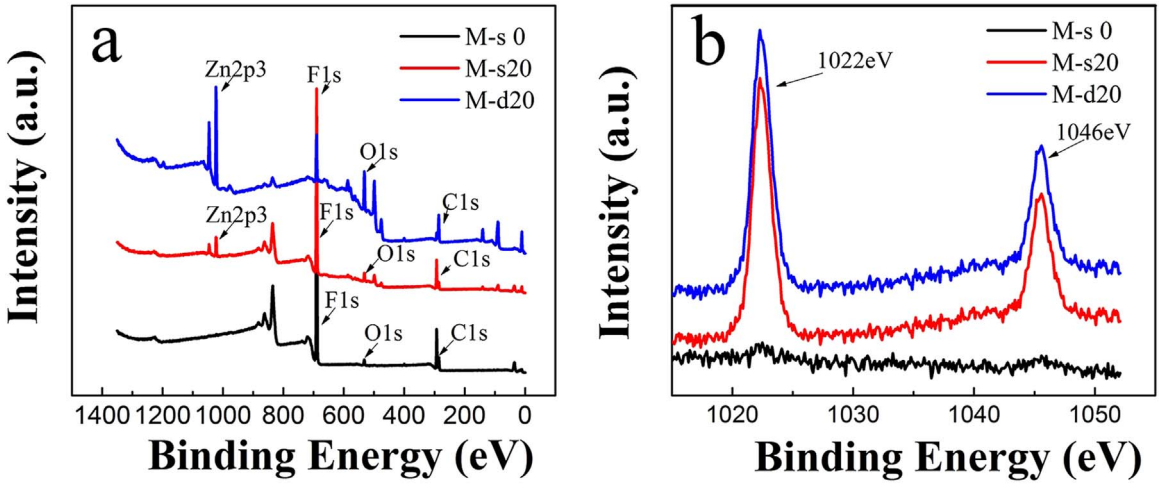

Fig. 7. XPS wide survey spectra (a) and Zn (2p) spectra (b).

under UV irradiation. The photocatalytic reusability of PTFE/ZnO membranes was also investigated (Fig. 9**d**). Under the same conditions, the decay rate of M-d20 for the removal efficiency of the RhB was faster than that of M-s20, which may because the ZnO particles immobilized on the surface of M-d20 by a two-step dipping and hydrothermal method are easier to fall off than those which were homogeneously immobilized on the surface of ultrafine PTFE. Ultimately, PTFE/ZnO membranes maintain the degradation efficiency to be 70% after five cycles, showing an excellent reusability. After UV irradiation, the break strength of the PTFE/ZnO membrane had no rapid changes (decreased slightly from 1.70 to 1.35 MPa) indicating that PTFE membranes have high UV resistance and oxidation resistance.

3.6. VMD tests with photo-degradation experiment

It is known that hydrophobicity and LEP value are an important properties for VMD. The formed hydrophobic surface attributes not only to the low surface energy but also to the roughness on multiple scales. Although ZnO has a high surface energy, the hydrophobicity of PTFE and the structure of nanofiber assembling are superior in improving hydrophobicity, which results in higher WCA and LEP values, as shown in Fig. 5 and Table 3. In addition, the low WCA and LEP caused by the dipping and sintering process made M-d20 unsuitable to bear the vacuum or pressure applied. So, M-s20 was chosen for further investigation.

VMD experiments were carried out with feed solution (1.5 L) containing 20 ppm RhB and 3.5 wt% NaCl. Results of the permeate flux and salt rejection were shown in Fig. 10. The permeation flux of the M-s20 and M-0 were measured for 15 h, respectively. It can be observed that the permeability of M-s20 was better than M-0 which is believed to be attributed to the open surface pore structure, and all the salt rejection values were above 99.5%. However, under the same VMD test conditions, the flux of membrane M-s20 was decreased from 16.26 to 14.91 L m^{-2}. h^{-1} after 6 h test which is much faster than M-s0 due to serious membrane fouling. The reasons can be concluded that, the RhB was more likely to be adsorbed on the surface of M-s20 because of ZnO. The accumulation of dye particles on the membrane surface and inside the membrane pores, forming a cake layer caused the membrane fouling. These pollutants may affect the wetting resistance and the partial pore wetting, which facilitated salt transportation in the next operation. As illustrated in Fig. 10**b**, M-s20 could effectively degrade dye in the feed solution with UV irradiation during VMD experiments and the dye removal rate of feed solution was up to 45% after 10 h operating time.

3.7. Characterization of self-cleaning of PTFE/ZnO membrane

UV irradiation and ZnO photocatalysis exhibit excellent photocatalytic property due to the production of strong hydroxyl radical which can degrade most of the complex organic compounds. Membrane fouling resulted from adhesion of pollutants to the membrane surface and subsequent blocking of membrane pores was also observed (Fig. 11). After 6-h VMD experiment, fouled membranes were immersed in distilled water and irradiated for 3 h by a UV light to recover the membrane flux, which was used as a membrane cleaning method. After a 3-h irradiation, the surface of fouled PTFE/ZnO membrane became much less polluted, indicating that the effect of photocatalysis on ZnO-loaded membrane provided PTFE/ZnO membrane a self-cleaning property. This further implies that UV irradiation might be an effective membrane cleaning method.

In order to further investigate self-cleaning property of PTFE/ZnO membrane, permeate flux recovery of PTFE/ZnO membrane after UV

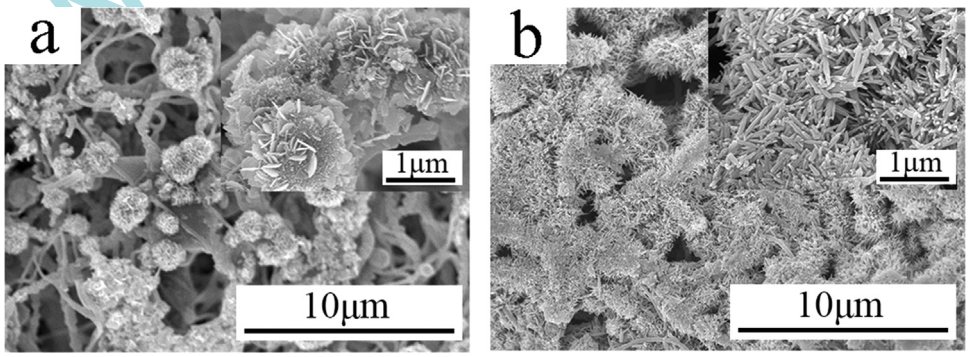

Fig. 8. Morphologies of PTFE/ZnO membranes (a: M-s20; b: M-d20; 5000×surface; 30000×surface).

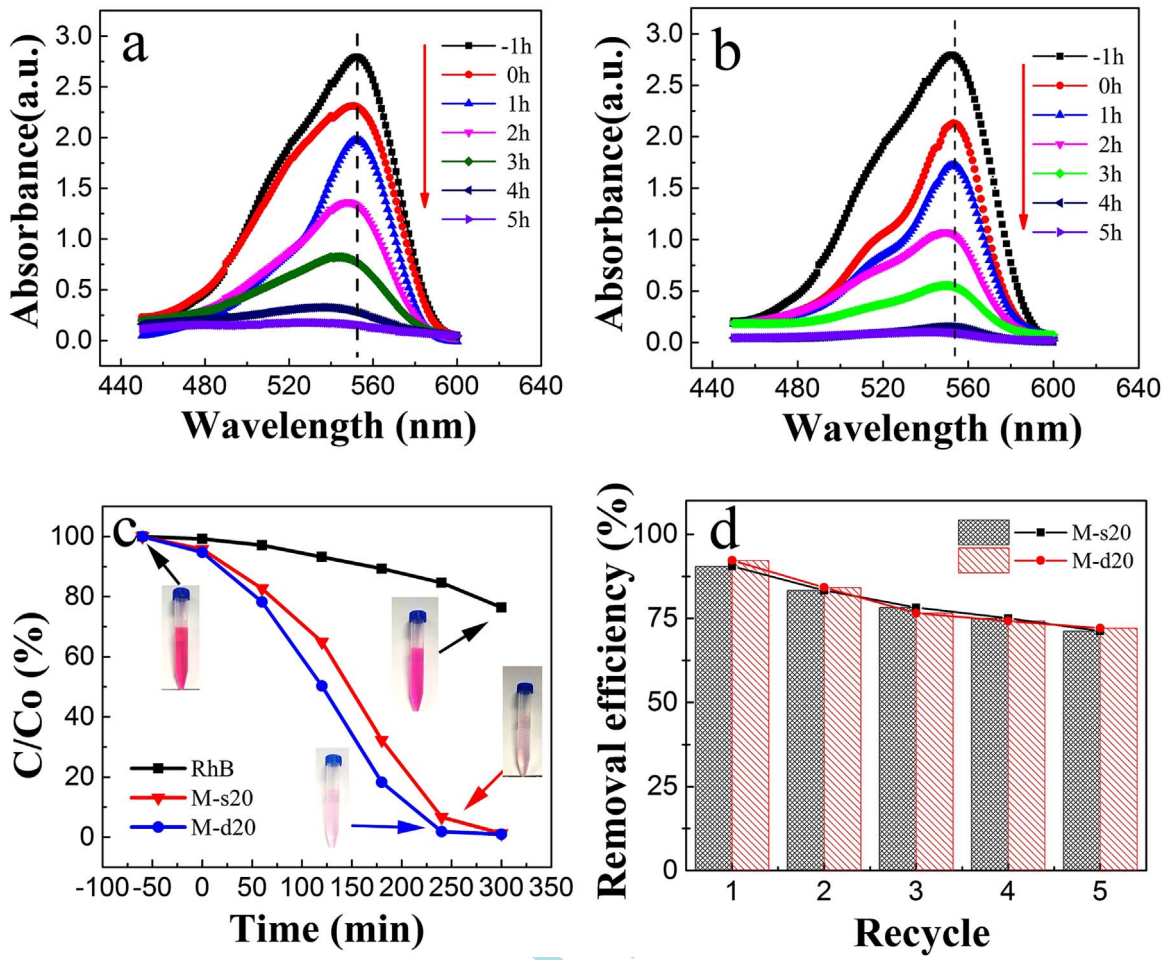

Fig. 9. The efficiency of photocatalytic degradation of RhB using PTFE/ZnO membranes (a: M-s20; b: M-d20; c: RhB degradation curves) under UV irradiation and the reusability after several cycles (d).

irradiation was explored, and the results of flux recovery vs. operating time are shown in Fig. 12. The flux recovery is a ratio of J (permeate flux of fouled membrane after 3 h UV irradiation) to J_0 (permeate flux of new membrane). It is shown that the permeate flux recovery rate could also reach higher than 94% (recovered flux was from 14.86 to 15.48 L m^{-2} h^{-1}) in the first 1 h of operating time after 3-h UV irradiation cleaning and the permeate flux recovery rate could reach to above 88%. All the salt rejection values were measured to be higher than 99.5%, suggesting that the photocatalytic cleaning was efficient.

4. Conclusion

Ultrafine fibrous PTFE/ZnO porous membranes were fabricated by sintering electrospun PTFE/PVA/zinc acetate dehydrate composite membranes to increase the uniform dispersion for the catalysts and obtain satisfactory recycling or reuse processes. Electrospun PTFE membranes exhibited a high specific surface area, excellent durability, and flexibility. The photocatalyst of ZnO particles was homogeneously immobilized on the surface of ultrafine PTFE fibers. PTFE/ZnO

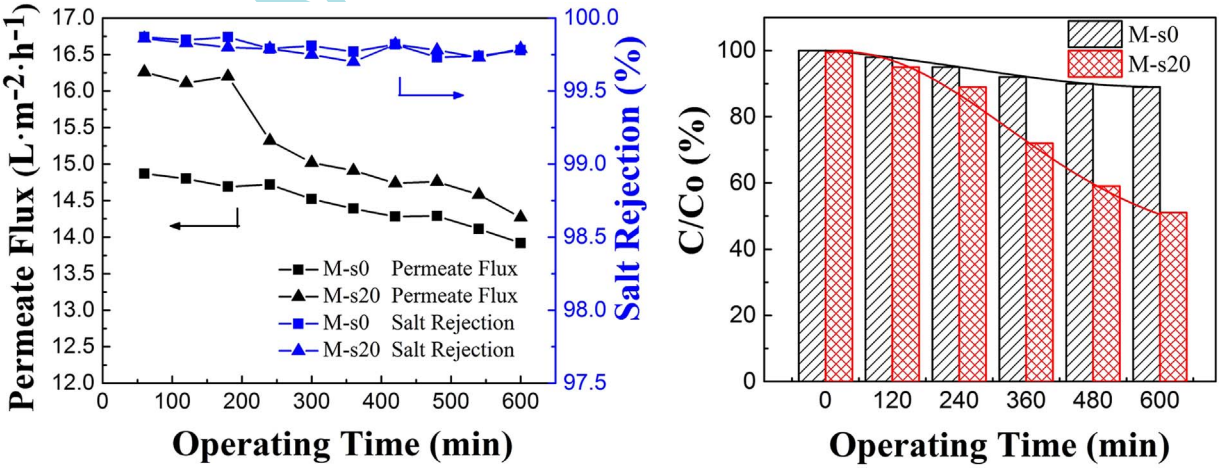

Fig. 10. Permeate flux and rejection in VMD experiments (a) and color removal rate of feed solution (b).

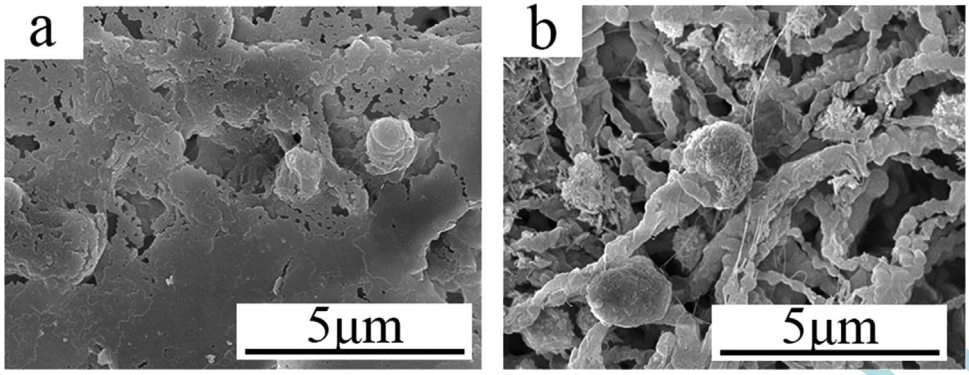

Fig. 11. SEM images of fouled PTFE/ZnO membranes before (a) and after UV irradiation (b).

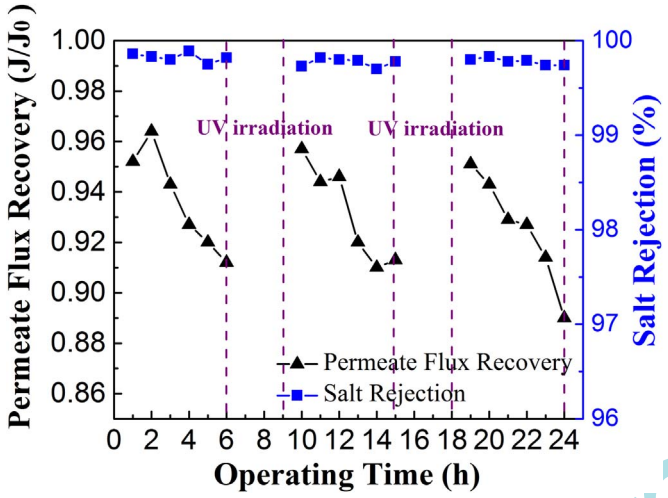

Fig. 12. The rejection and permeate flux recovery of self-cleaning PTFE/ZnO membrane in VMD experiments with three times UV irradiation (M-s20).

membranes showed a high removal efficiency up to 97% for the RhB degradation after 5 h under UV light. The degradation rate remained above 70% after 5 cycles, indicating that these membranes possessed a higher UV and oxidation resistance. VMD experiments indicated that appropriate PTFE/ZnO membranes could be an effective way for better salt rejection and dye removal at the same time. The fouled PTFE/ZnO membranes can be cleaned with UV irradiation, showing a good self-cleaning ability. Results from this study suggest potential applications of PTFE/ZnO in the treatment of water contaminated with organic compounds.

Acknowledgments

This work was supported by National Natural Science Foundation of China (No. 21404079), Tianjin Municipal University Science and Technology Development Fund Project (Grant No. TJ 20140306), The Science and Technology Plans of Tianjin (No. 15PTSYJC00240), the Program for Changjiang Scholars and Innovative Research Team in University (PCSIRT) of Ministry of Education of China (No. IRT13084).

Appendix A. Supplementary material

Supplementary data associated with this article can be found in the online version at http://dx.doi.org/10.1016/j.memsci.2017.04.015.

References

[1] I. Ali, V.K. Gupta, Advances in water treatment by adsorption technology, Nat. Protoc. 1 (2006) 2661–2667.
[2] O. Legrini, E. Oliveros, A. Braun, Photochemical processes for water treatment, Chem. Rev. 93 (1993) 671–698.
[3] J. Mu, C. Shao, Z. Guo, Z. Zhang, M. Zhang, P. Zhang, B. Chen, Y. Liu, High photocatalytic activity of ZnO– carbon nanofiber heteroarchitectures, ACS Appl. Mater. Interfaces 3 (2011) 590–596.
[4] B. Nicolaisen, Developments in membrane technology for water treatment, Desalination 153 (2003) 355–360.
[5] X. Zhang, T. Zhang, J. Ng, D.D. Sun, High-performance multifunctional TiO2 nanowire ultrafiltration membrane with a hierarchical layer structure for water treatment, Adv. Funct. Mater. 19 (2009) 3731–3736.
[6] M. Khayet, Membranes and theoretical modeling of membrane distillation: a review, Adv. Colloid Interface Sci. 164 (2010) 56–88.
[7] A. Criscuoli, P. Bafaro, E. Drioli, Vacuum membrane distillation for purifying waters containing arsenic, Desalination 323 (2013) 17–21.
[8] J.W. Chen, Y.Q. Zhang, Y.F. Wang, X.S. Ji, L. Zhang, X.G. Mi, H. Huang, Removal of inhibitors from lignocellulosic hydrolyzates by vacuum membrane distillation, Bioresour. Technol. 144 (2013) 680–683.
[9] L.D. Tijing, C.W. Yun, J.S. Choi, S. Lee, S.H. Kim, H.K. Shon, Fouling and its control in membrane distillation – a review, J. Membr. Sci. 475 (2015) 215–244.
[10] J.R. Du, S. Peldszus, P.M. Huck, X. Feng, Modification of membrane surfaces via microswelling for fouling control in drinking water treatment, J. Membr. Sci. 475 (2015) 488–495.
[11] J. Grzechulskadamszel, M. Tomaszewska, A.W. Morawski, Integration of photo-catalysis with membrane processes for purification of water contaminated with organic dyes, Desalination 156 (2010) 295–300.
[12] D. Hou, G. Dai, H. Fan, H. Huang, J. Wang, An ultrasonic assisted direct contact membrane distillation hybrid process for desalination, J. Membr. Sci. 476 (2015) 59–67.
[13] Q.-l. Huang, C.-f. Xiao, X.-y. Hu, A novel method to prepare hydrophobic poly (tetrafluoroethylene) membrane, and its properties, J. Mater. Sci. 45 (2010) 6569–6573.
[14] K.-i. Kurumada, T. Kitamura, N. Fukumoto, M. Oshima, M. Tanigaki, S.-i. Kanazawa, Structure generation in PTFE porous membranes induced by the uniaxial and biaxial stretching operations, J. Membr. Sci. 149 (1998) 51–57.
[15] H. Zhu, H. Wang, F. Wang, Y. Guo, H. Zhang, J. Chen, Preparation and properties of PTFE hollow fiber membranes for desalination through vacuum membrane distillation, J. Membr. Sci. 446 (2013) 145–153.
[16] J.H. Carey, J. Lawrence, H.M. Tosine, Photodechlorination of PCB's in the presence of titanium dioxide in aqueous suspensions, Bull. Environ. Contam. Toxicol. 16 (1976) 697–701.
[17] S. Yurdakal, G. Palmisano, V. Loddo, V. Augugliaro, L. Palmisano, Nanostructured rutile TiO2 for selective photocatalytic oxidation of aromatic alcohols to aldehydes in water, J. Am. Chem. Soc. 130 (2008) 1568–1569.
[18] K. Hashimoto, H. Irie, A. Fujishima, TiO2 photocatalysis: a historical overview and future prospects, Jpn. J. Appl. Phys. 44 (2005) 8269.
[19] A. Fujishima, Electrochemical photolysis of water at a semiconductor electrode, nature 238 (1972) 37–38.
[20] S. Mozia, Photocatalytic membrane reactors (PMRs) in water and wastewater treatment. A review, Sep. Purif. Technol. 73 (2010) 71–91.
[21] S. Mozia, K. Szymański, B. Michalkiewicz, B. Tryba, M. Toyoda, A.W. Morawski, Effect of process parameters on fouling and stability of MF/UF TiO 2 membranes in a photocatalytic membrane reactor, Sep. Purif. Technol. 142 (2015) 137–148.
[22] A. Bozzi, T. Yuranova, J. Kiwi, Self-cleaning of wool-polyamide and polyester textiles by TiO 2-rutile modification under daylight irradiation at ambient temperature, J. Photochem. Photobiol. A: Chem. 172 (2005) 27–34.
[23] B. Sankapal, M.C. Lux-Steiner, A. Ennaoui, Synthesis and characterization of anatase-TiO 2 thin films, Appl. Surf. Sci. 239 (2005) 165–170.
[24] C.C. Pei, W.W.-F. Leung, Enhanced photocatalytic activity of electrospun TiO 2/ZnO nanofibers with optimal anatase/rutile ratio, Catal. Commun. 37 (2013) 100–104.
[25] S. Singh, H. Mahalingam, P.K. Singh, Polymer-supported titanium dioxide photo-catalysts for environmental remediation: a review, Appl. Catal. A: Gen. 462–463 (2013) 178–195.
[26] M. Bognitzki, W. Czado, T. Frese, A. Schaper, M. Hellwig, M. Steinhart, A. Greiner, J.H. Wendorff, Nanostructured fibers via electrospinning, Adv. Mater. 13 (2001) 70–72.
[27] S. Nataraj, B. Kim, J. Yun, D. Lee, T. Aminabhavi, K. Yang, Electrospun

nanocomposite fiber mats of zinc-oxide loaded polyacrylonitrile, Carbon Lett. 9 (2008) 108–114.
[28] N. Olaru, G. Calin, L. Olaru, Zinc oxide nanocrystals grown on cellulose acetate butyrate nanofiber mats and their potential photocatalytic activity for dye degradation, Ind. Eng. Chem. Res. 53 (2014) 17968–17975.
[29] J. Shen, Y.-n. Wu, L. Fu, B. Zhang, F. Li, Preparation of doped TiO2 nanofiber membranes through electrospinning and their application for photocatalytic degradation of malachite green, J. Mater. Sci. 49 (2014) 2303–2314.
[30] P. Samanta, S. Bagchi, S. Mishra, Synthesis and sensing characterization of ZnO nanofibers prepared by electrospinning, Mater. Today.: Proc. 2 (2015) 4499–4502.
[31] H. Zhang, M. Yu, J. Zhang, C. Sheng, X. Yan, W. Han, Y. Liu, S. Chen, G. Shen, Y. Long, Fabrication and photoelectric properties of La-doped p-type ZnO nanofibers and crossed p–n homojunctions by electrospinning, Nanoscale 7 (2015) 10513–10518.
[32] Y. Huang, Q.-L. Huang, H. Liu, C.-X. Zhang, Y.-W. You, N.-N. Li, C.-F. Xiao, Preparation, characterization, and applications of electrospun ultrafine fibrous PTFE porous membranes, J. Membr. Sci. 523 (2017) 317–326.
[33] Y. Zhang, M.K. Ram, E.K. Stefanakos, D.Y. Goswami, Synthesis, characterization, and applications of ZnO nanowires, J. Nanomater. 2012 (2012) 1–22.
[34] C.-C. Lin, Y.-Y. Li, Synthesis of ZnO nanowires by thermal decomposition of zinc acetate dihydrate, Mater. Chem. Phys. 113 (2009) 334–337.
[35] J. Duan, X. Huang, E. Wang, PEG-assisted synthesis of ZnO nanotubes, Mater. Lett. 60 (2006) 1918–1921.
[36] A. Gugliuzza, E. Drioli, PVDF and HYFLON AD membranes: ideal interfaces for contactor applications, J. Membr. Sci. 300 (2007) 51–62.
[37] Z. Tao, Y. Yao, R. Xiang, Y. Wu, Formation and characterization of polytetrafluoroethylene nanofiber membranes for vacuum membrane distillation, J. Membr. Sci. 453 (2014) 402–408.
[38] S. Zhao, Y. Yao, C. Ba, W. Zheng, J. Economy, P. Wang, Enhancing the performance of polyethylenimine modified nanofiltration membrane by coating a layer of sulfonated poly(ether ether ketone) for removing sulfamerazine, J. Membr. Sci. 492 (2015) 620–629.
[39] H.J. Cho, C.S. Ki, H. Oh, K.H. Lee, I.C. Um, Molecular weight distribution and solution properties of silk fibroins with different dissolution conditions, Int. J. Biol. Macromol. 51 (2012) 336–341.
[40] H.J. Kim, I.C. Um, Relationship between rheology and electro-spinning performance of regenerated silk fibroin prepared using different degumming methods, Korea-Aust. Rheol. J. 26 (2014) 119–125.
[41] Z.-M. Huang, Y.-Z. Zhang, M. Kotaki, S. Ramakrishna, A review on polymer nanofibers by electrospinning and their applications in nanocomposites, Compos. Sci. Technol. 63 (2003) 2223–2253.
[42] K. Yoon, H.N. Lee, C.S. Ki, D. Fang, B.S. Hsiao, B. Chu, I.C. Um, Effects of degumming conditions on electro-spinning rate of regenerated silk, Int. J. Biol. Macromol. 61 (2013) 50–57.
[43] C.C. Lin, Y.Y. Li, Synthesis of ZnO nanowires by thermal decomposition of zinc acetate dihydrate, Mater. Chem. Phys. 113 (2009) 334–337.
[44] B. Liu, H.C. Zeng, Hydrothermal synthesis of ZnO nanorods in the diameter regime of 50 nm, J. Am. Chem. Soc. 125 (2003) 4430–4431.
[45] M. Mehrabian, R. Azimirad, UV detecting properties of hydrothermal synthesized ZnO nanorods, Phys. E Low-Dimens. Syst. Nanostruct. 43 (2011) 1141–1145.
[46] S. Varanasi, Z.-X. Low, W. Batchelor, Cellulose nanofibre composite membranes–Biodegradable and recyclable UF membranes, Chem. Eng. J. 265 (2015) 138–146.